Surface Energy and Wettability Study of Flip Chip Packaging Materials

Jinlin Wang
Assembly Test and Technology Development
Intel Corporation
5000 W. Chandler Blvd., Chandler, AZ 85226, U.S.A.

Abstract

The surface energy of solid surfaces and surface tension of liquids are important parameters in the IC package assembly process. Wettability analyses have been completed for various materials used in the assembly process of flip chip packages, including underfills, substrates, fluxes, and lead free solders. We will highlight some of these results in this paper. We will focus our discussion on substrate surface energy analysis. A brief discussion of different surface energy methods and the liquid selection criteria will be given. The advantage and limitation of the surface energy calculation methods will be discussed. The data from several case studies will be presented. Our results show that contact angle and surface energy measurements are very useful for quality control and product development where interfacial properties are important.

Key words: contact angle, surface energy, flip chip, substrate, underfill, and flux.

Introduction

In flip-chip packaging, a flux material is deposited on the bump area of the substrate and a die is attached on the substrate. The package undergoes a reflow process to interconnect the die with the substrate. An underfill is dispensed on one or two adjacent sides of the die. The underfill is driven by capillary force to fill the gap between the die and substrate. The application of an underfill reduces the stress on solder bumps and enhances the reliability of the solder joints.

Contact angle, surface tension, and viscosity are some of the key factors affecting flux performance in die attach process and underfill flow [1]. The wetting of substrate, solder bump, and die surfaces by flux and underfill depends on the relative surface energies of these materials. Non-wetting of the flux and underfill is one of the issues that need too be considered in the flip chip assembly process. For an established process, the consistency of substrate surface is very important; on the other hand, a liquid flux or underfill with higher surface energy would spread less over a solid surface, which could result in poor wetting at the interface.

There are several methods for surface energy measurements. One of the methods for solid surface energy measurement is the inverse gas chromatography (IGC) method [2]. The dispersive component of free energy is obtained by measuring the retention time of a series of alkenes and the polar component of free energy is obtained by measuring the retention time of a series of polar liquids. The IGC method can measure the surface energy at elevated temperatures. However, it is time consuming and the sample surface needs to be a homogeneous material. Another method for surface energy measurement is atomic force microscopy (AFM). In this method, the work of adhesion is obtained from a pull-off test [3]. The sample for an AFM test usually needs to be moisture free and the probe tip needs to be coated with the same material as the solid surface in order to find the surface energy of the solid, which is hard to do in many cases.

A dynamic contact angle system can be used for surface energy characterization of solid surfaces. The measurements are used for both materials and process characterizations, as well as for failure analysis. There are several papers [4-6], which discuss the applications of contact angle measurement to wafer manufacturing processes, surface cleaning, contamination level, and surface modification. Surface energy can be calculated from contact angle data using a two or three-liquid method. The surface energy data can then be used to correlate with the performance of materials in assembly process.

In this paper, we will discuss some of the applications of a video contact angle system for contact angle and surface energy measurements of flip chip packages. Three probing liquids: DI water, methylene iodide, and glycerol are used in contact angle measurements and surface energy calculations for different substrates. The different surface energy calculation methods are reviewed. The advantage and

limitation of each surface energy method are discussed in details. Also, the contact angles of fluxes and underfills on substrates are measured. The correlation between the surface energy and flux and underfill contact angle are also studied. The interfacial properties between the underfill and substrate are important to the integrity of the package. The consistency of substrate surface is critical for the quality of the packages. The contamination of substrate surfaces can increase the contact angle and cause de-wetting problem in chip attach and underfill processes. The effect of cleanliness of substrate on the contact angle is investigated. The clean surface has much smaller contact angle than the unclean surface. Contact angle measurements are used to analyze the impact of flux residue on the wetting of substrates. We will discuss the impact of contact angle and surface energy analysis.

Method for Surface Energy Calculation

The force balance on a sessile drop of liquid on a solid is given by Young's equation:

$$\gamma_{SV} = \gamma_{SL} + \gamma_{LV}\cos\theta \tag{1}$$

where γ_{LV} is the surface tension of liquid at liquid-vapor interface, γ_{SL} the surface tension of solid at solid-liquid interface, and γ_{SV} the surface tension of solid at solid-vapor interface. The free energy, ΔG_{SL}, and work of adhesion, W_{SL}, at solid and liquid interface are given by:

$$\Delta G_{SL} = -W_{SL} = \gamma_{SL} - \gamma_{SV} - \gamma_{LV} \tag{2}$$

Combining with Young's equation, one has:

$$\Delta G_{SL} = -W_{SL} = -\gamma_{LV}\left(1+\cos\theta\right) \tag{3}$$

where θ is the contact angle. The surface energy can be separated into polar component, γ^p, and dispersive component, γ^d, so that:

$$\gamma = \gamma^d + \gamma^p \tag{4}$$

In the geometric mean method [7], it was assumed that the free energy of adhesion is equal to the geometric mean of free energy of solid and liquid. Applying geometric mean method in Young's equation, one has:

$$\left(1+\cos\theta_1\right)\gamma_1 = 2\left[\sqrt{\gamma_1^d\gamma_s^d} + \sqrt{\gamma_1^p\gamma_s^p}\right] \tag{5}$$

$$\left(1+\cos\theta_2\right)\gamma_2 = 2\left[\sqrt{\gamma_2^d\gamma_s^d} + \sqrt{\gamma_2^p\gamma_s^p}\right] \tag{6}$$

In the three-liquid method [8, 9], it was assumed that the surface energy had two components, apolar and acid-base:

$$\gamma_{ij} = \gamma_{ij}^{LW} + \gamma_{ij}^{AB} \tag{7}$$

and

$$\Delta G_{ij}^{AB} = -2\left(\sqrt{\gamma_i^+\gamma_j^-} + \sqrt{\gamma_i^-\gamma_j^+}\right) \tag{8}$$

where superscripts LW, AB, +, and - refer to apolar, acid-base, acid, and base components, respectively. Combining the three liquid method with Young's equation, one has:

$$\frac{\left(1+\cos\theta_1\right)\gamma_1}{2} = \sqrt{\gamma_s^{LW}\gamma_1^{LW}} + \sqrt{\gamma_s^+\gamma_1^-} + \sqrt{\gamma_s^-\gamma_1^+} \tag{9}$$

$$\frac{\left(1+\cos\theta_2\right)\gamma_2}{2} = \sqrt{\gamma_s^{LW}\gamma_2^{LW}} + \sqrt{\gamma_s^+\gamma_2^-} + \sqrt{\gamma_s^-\gamma_2^+} \tag{10}$$

$$\frac{\left(1+\cos\theta_3\right)\gamma_3}{2} = \sqrt{\gamma_s^{LW}\gamma_3^{LW}} + \sqrt{\gamma_s^+\gamma_3^-} + \sqrt{\gamma_s^-\gamma_3^+} \tag{11}$$

Rewriting the above equation in a matrix form, one has

$$\mathbf{AX=B} \tag{12}$$

Where

$$A = \begin{pmatrix} \sqrt{\gamma_1^{LW}} & \sqrt{\gamma_1^+} & \sqrt{\gamma_1^-} \\ \sqrt{\gamma_2^{LW}} & \sqrt{\gamma_2^+} & \sqrt{\gamma_2^-} \\ \sqrt{\gamma_3^{LW}} & \sqrt{\gamma_3^+} & \sqrt{\gamma_3^-} \end{pmatrix}$$

$$B = \begin{pmatrix} \frac{(1+\cos\theta_1)\gamma_1}{2} \\ \frac{(1+\cos\theta_2)\gamma_2}{2} \\ \frac{(1+\cos\theta_3)\gamma_3}{2} \end{pmatrix}$$

$$X = \begin{pmatrix} \sqrt{\gamma_s^{LW}} \\ \sqrt{\gamma_s^-} \\ \sqrt{\gamma_s^+} \end{pmatrix}$$

The coefficient matrix **A** tends to be ill conditioned if its condition number is large [10]. In this case, the experimental error for the contact angle will have a large impact on the surface energy result. The three liquids chosen for the surface energy measurements should have a small condition number for the coefficient matrix.

The matrix norm is needed for the condition number calculation. The matrix norm is defined as

$$\|A\|_\infty = \max_{1<j<m} \sum_{j=1}^{n} |A_{ij}| \qquad (13)$$

The condition number of the coefficient matrix is defined as

$$Cond(A) = \|A\|_\infty \|A^{-1}\| \qquad (14)$$

In the three-liquid method, three probing liquids are needed in order to solve three unknowns – aploar, acid, and base components of solid surface. The surface tension and its components for these probing liquids are listed in Table 1. The condition numbers for some liquid triplets are listed in Table 2

Table 1. Surface energetic parameters of probing liquids. The unit is dyne/cm.

	WA	MI	GL	FA	EG	DD
γ	72.8	50.8	64	58	47.7	25.4
γ^d	22.1	48.5	N/A	39.5		
γ^p	50.7	2.3	N/A	18.7		
γ^{LW}	21.8	50.8	33	39	29	25.4
γ^+	25.5	0	3.92	2.28	1.92	0
γ^-	25.5	0	57.4	39.6	47	0

Legend: WA=water; MI=methylene iodide; GL=glycerol; FA= formamide; EG=ethylene glycol; DD= dodecane.

Table 2. Condition number for liquid triplets

liquid triplet	Condition number
WA-MI-GL	7.3
WA-EG-GL	161.6
WA-DD-GL	7.5
WA-DD-FA	7.2
WA-GL-FA	20.3
WA-EG-FA	22.7
GL-EG-FA	75.5
GL-MI-FA	234.4

Usually, a liquid triplet with dispersive, acid, and basic liquids has a low condition number. We chose DI water, methylene iodide, and glycerol as probing liquids for the acid and base method.

Experimental

A video contact angle system was used with a 100 ul glass barrel syringe with TPFE tipped stainless steel plunger and a stainless steel needle for surface energy measurement. The dispensing volume was controlled by a motorized syringe dispensing system. A substrate was placed onto the stage and adjusted to have the desired measurement spot right below the syringe needle. A drop of liquid with controlled volume was dispensed to form a pedant drop on the needle tip. The substrate was raised until it touches the liquid drop, then the substrate was lowered until the droplet separated from the needle tip. The image of droplet on the substrate was captured after it was pulled down from needle tip, using video image processing software. The contact angle can be calculated, using the image processing software.

For contact angle measurement of flux and underfill materials on substrates at high temperature, a heated environmental chamber was used. Dynamic contact angle was captured to get images from 0 to 120 seconds at 5 frame/min sampling rate for time dependent underfill contact angle at 1100^{o}C. The advantage of using an optical based technique with single liquid drop for contact angle is the small volume used, which can minimize the curing of material at elevated temperatures.

An actual image of a DI water drop on poor and good wetting surfaces is shown in Fig. 1. Since the underfill material has fillers, it is viscoelastic. The underfill drop will spread with time. Fig. 2 shows the contact angle of an underfill material on a glass

surface at 0, 12, and 120 sec at 110°C. The incomplete fillet on a package as shown in Fig. 3 and underfill non- wet as shown in Fig. 4 are two major issues in the underfill process.

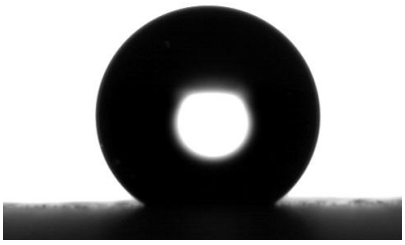

(a)

(b)

Fig. 1. DI water contact angle on poor (a) and good (b) wetting surfaces.

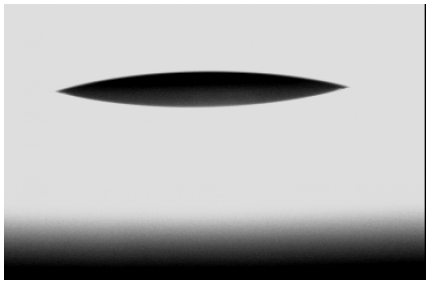

(a)

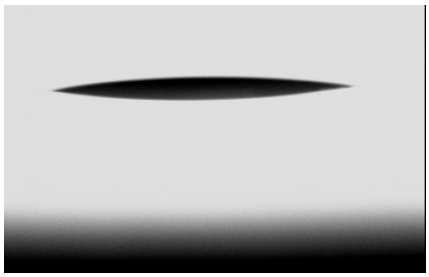

(b)

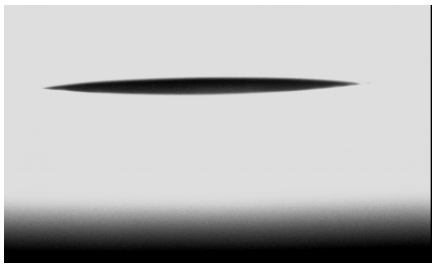

(c)

Fig. 2. The contact angle of an underfill material on a glass surface at 0 (a), 12 (b), and 120 (c) sec at 110°C.

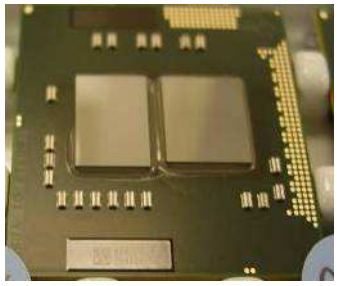

Fig. 3. Incomplete fillet.

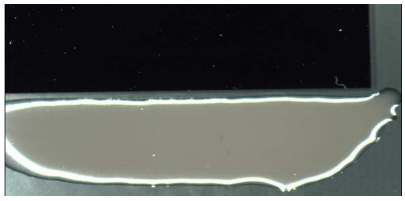

(a)

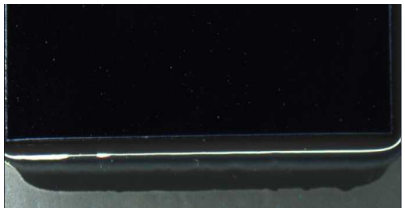

(b)

Fig. 4. Non wet (a) and good (b) units.

Results and Discussions

There are two issues with the surface energy calculation methods by contact angle measurements. The models can yield a negative square root of surface energy component for certain contact angle

data [10, 11]. This can be due to the experiment error from contact angle measurement. From data published in the literature and the data we collected, it was concluded that the experiment error is not the only factor for the negative value. Fig. 5 shows the relationship between the surface energy component and the contact angle. This is calculated using geometric mean method with water and methylene iodide contact angle from 0 to 180 degree. The graph is divided into three regions by the sign of the square root of the surface energy components. The top left region has negative dispersive component. In this region, the contact angle of methylene iodide is over 100 degrees and is higher than the water contact angle. Since water usually has a higher contact angle than methylene iodide, it is very unlikely to have negative dispersive component from experimental data. The middle region gives both positive dispersive and polar components. The bottom left region gives negative polar component. Sometimes experimental data can give negative polar component. The surface energy should decrease with an increase in contact angle. Table 3 shows that a pair of high contact angles gives high surface energy with the geometric mean method. Fig. 6 shows the surface energy as a function of water contact angle when methylene iodide contact angle is 41 degrees. For a fixed methylene iodide contact angle in the geometric mean method, the surface energy first decreases with water contact angle to a minimum surface energy. Then the surface energy increases with water contact angle. This is before the polar component becomes negative. Fig. 7 shows the region of high contact angles with high surface energy.

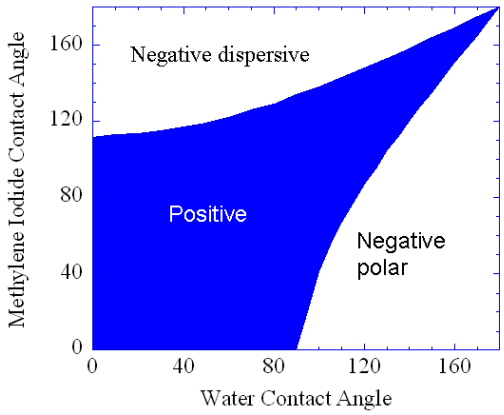

Fig. 5. Relationship between surface components and the contact angle for the geometric mean method.

Table 3. A pair of high contact angles gives high surface energy with the geometric mean method.

Water contact angle	86	100
MI contact angle	41	42
Dispersive	37	40.2
Polar	2.1	0
Surface energy	39.1	40.2

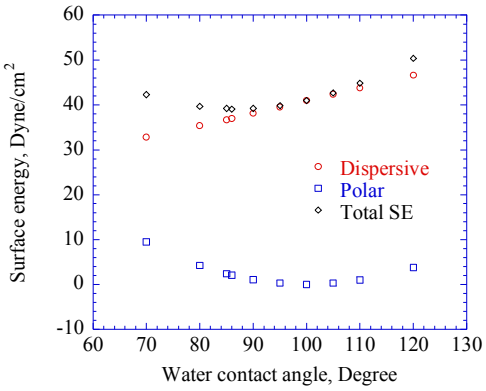

Fig. 6. The surface energy as a function of water contact angle when methylene iodide contact angle is 41 degrees.

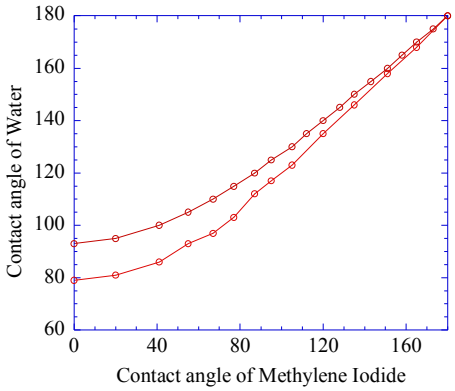

Fig. 7. The region of high contact angles with high surface energy.

For the acid base method with three liquids, it also shows negative components. It happens more often and is more complicated than the geometric mean method. Fig. 8 shows the relationship between the square root of surface energy components and the

contact angle for acid and base method. The part with data points in Fig. 8 gives positive surface energy components. Fig. 9 shows the positive surface energy component region when the contact angle of glycerol is 75 degree. Table 4 shows a triplet of high contact angles gives high surface energy with acid base method. Fig. 10 shows the surface energy as a function of water contact angle when methylene iodide and glycerol contact angles are 40 and 75 degrees, respectively.

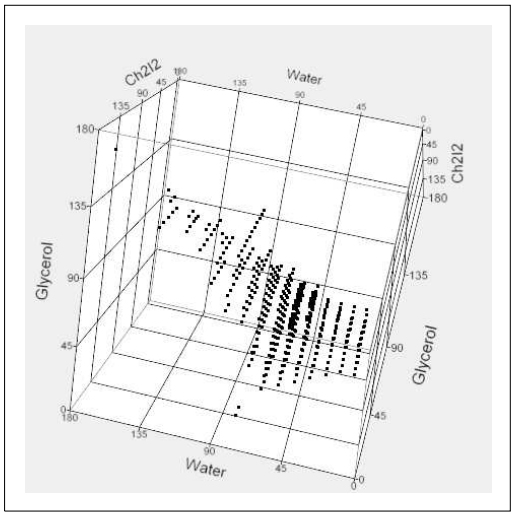

Fig. 8. Relationship between square root of surface components and the contact angle for the acid and base method.

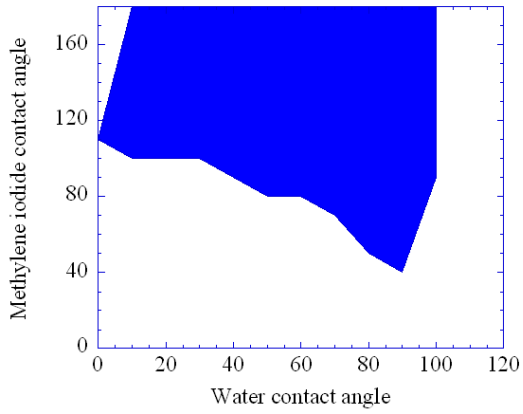

Fig. 9. The positive surface energy component region when the contact angle of glycerol is 75 degree.

Table 4. A triplet of high contact angles gives high surface energy for acid base method.

Water contact angle	80	82
MI contact angle	55	57
GL contact angle	44	55
Dispersive	31.4	30.3
SQRT(A)	8	4.7
SQRT(B)	0.2	0.9
Surface energy	34	34.5

The polar component of the surface energy in the geometric mean and acid base methods is usually small compared with the dispersive component. If the negative component is close to zero, its contribution to the total surface energy is negligible. There are several ways for treating the negative square root of the surface energy. One is to square it so it becomes positive. The second approach is to take the negative sign after squaring it and subtract the negative part from the equation. The third approach is to take the negative component as zero. We consider it as positive in our calculation since it does not occur frequently and the negative number is small in most cases.

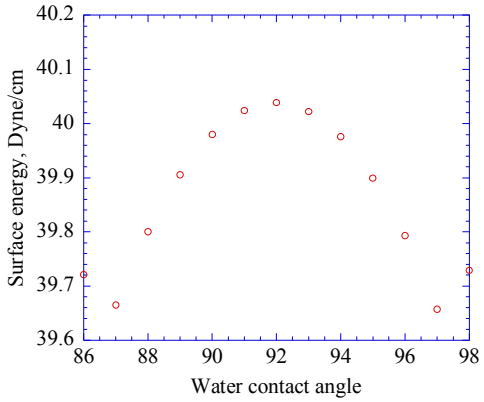

Fig. 10. The surface energy as a function of water contact angle when methylene iodide and glycerol contact angles are 40 and 75 degree, respectively.

The work of adhesion between two solid surfaces can be determined by the following equation,

$$W_A = 2\left[\sqrt{\gamma_{S1}^{d}\gamma_{S2}^{d}} + \sqrt{\gamma_{S1}^{p}\gamma_{S2}^{p}}\right] \qquad (15)$$

$$W_A = 2\sqrt{\gamma_{S1}^{LW}\gamma_{S2}^{LW}} + 2\sqrt{\gamma_{S1}^{+}\gamma_{S2}^{-}} + 2\sqrt{\gamma_{S1}^{-}\gamma_{S2}^{+}} \qquad (16)$$

Surface energy for solid and solid interface predicts the work of adhesion, the work needed to separate them from adhesion. For liquid and solid interface, it predicts the spread of the liquid on the solid surface.

Material T is a cover tape material and it is in contact with the material M. In order to prevent the tape material from sticking to material M, both the surface energy of the tape and the work of adhesion between the two need to be low. The surface energy for two M and four T materials is shown in Tables 5 and 6. Table 7 shows the work of adhesion for different solid interfaces. The tapes with low surface energy give low work of adhesion and the interfaces with low work of adhesion are less sticky.

Table 5. Surface energy by the geometric mean method for different solid surfaces.

Material	Dispersive	Polar	Surface Energy
M1	33.8	5.6	39.4
M2	37.9	5.4	43.3
T1	32.7	7.7	40.5
T2	12.7	0.7	13.4
T3	34.6	13.4	48.0
T4	12.1	0.5	12.6

Table 6. Surface energy by the acid base method for different solid surfaces.

Material	Dispersive	SQRT (Acid)	SQRT (Base)	Surface Energy
M1	38.2	0.9	3.9	45.0
M2	42.4	0.2	3.2	43.9
T1	38.2	0.1	3.6	39.0
T2	13.4	0.3	1.4	14.4
T3	42.6	0.2	4.4	44.0
T4	12.6	0.1	1.1	12.8

Table 7. Work of adhesion between two solid surfaces.

M	T	Wa from Geometric mean method	Wa from the acid and base method
1	1	79.7	81.3
1	2	45.3	49.8
1	3	85.7	86.2
1	4	43.8	47.0
2	1	83.4	83.5
2	2	47.7	50.9
2	3	89.5	88.5
2	4	46.2	48.3

The flux contact angle was measured at 0, 1, and 4 min. The flux contact angle on substrates was shown in Fig. 11. Substrate A had a high contact angle and it had die misalignment issue. The contact angle decreased with time. The contact angle difference between different substrates increased with time. Figs. 12 and 13 show the water and methylene iodide contact angle on the substrates, respectively. The water contact angle of substrate A and B are very similar and the methylene iodide contact angle of substrate B and C are very similar. Substrates B and C did not have a die misalignment issue. The water contact angle did not correlate with the substrate performance. Figs. 14 and 15 show the surface energy by the geometric mean and acid base methods. The surface energy by the geometric mean method had good correlation with substrate performance, while the surface energy by acid base method did not have good correlation. Unlike water, glycerol contact angle decreases with time due to its high viscosity as shown in Fig. 16. For surface energy calculation, the equilibrium contact angle needs to be used. The surface energy by the acid base method with glycerol contact angle at 4 min is very similar with the surface energy from the geometric mean method as shown in Fig. 17.

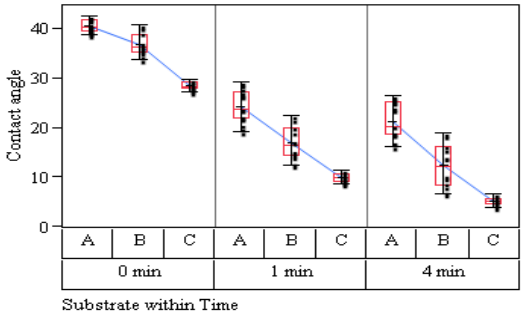

Fig. 11. The flux contact angle on substrates.

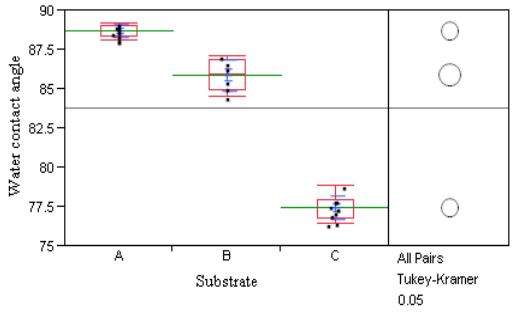

Fig. 12. The water contact angle on substrates.

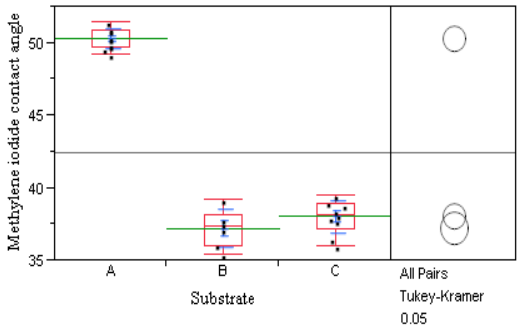

Fig. 13. The methylene iodide contact angle on substrates

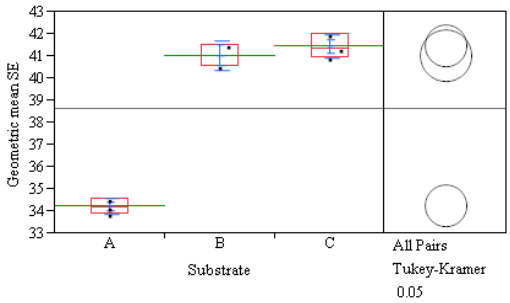

Fig. 14. Surface energy by the geometric mean method.

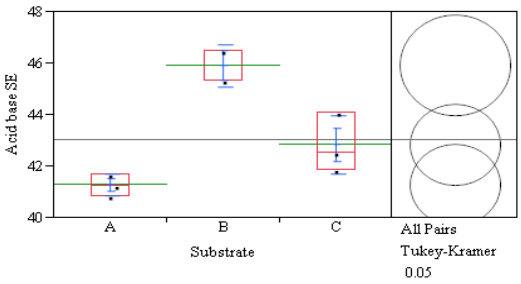

Fig. 15. Surface energy by the acid base method for different substrates with glycerol contact angle at 0 min.

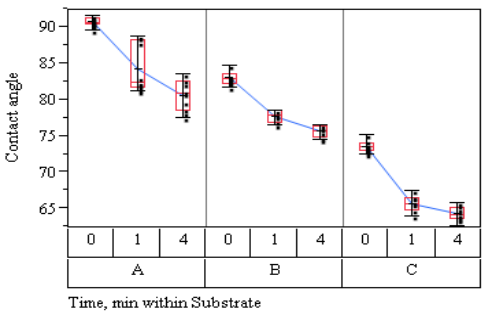

Fig. 16. Glycerol contact angle on substrates.

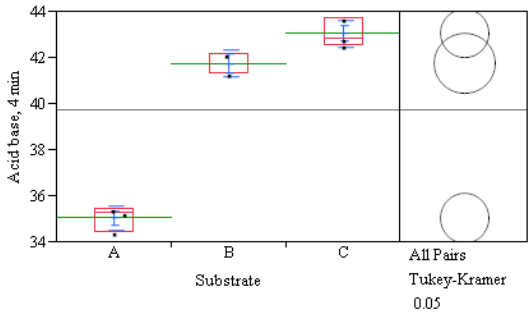

Fig. 17. Surface energy by the acid base method for different substrates with glycerol contact angle at 4 min.

Table 8 shows the surface energy for the units with incomplete underfill fillet. All the units have low surface energy. Fig. 18 shows the underfill contact angle on the units with incomplete fillet. Most units had very little underfill spread and high contact angle. It had a couple of units with good underfill spread and low contact angle after 30 sec. Low contact angle underfill drops have an oval shape from the top down view and the surface wettability is not homogenous.

Table 8. Surface energy by the geometric mean method for the packages with incomplete fillet.

	A	B	C	D	E	F
Dispersive	21	22	32	32	33	18
Polar	0.3	0.1	0.6	0.9	0.5	0.0
Surface Energy	22	22	33	33	33	18

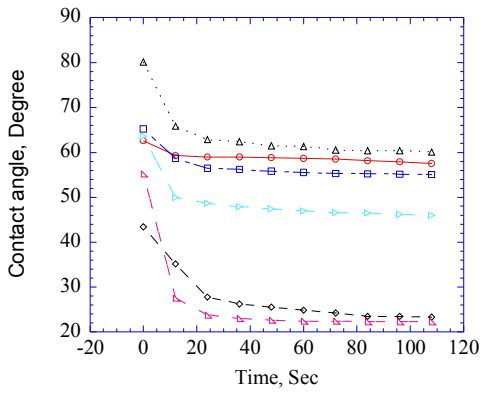

Fig.18. Underfill contact angle at 110C for incomplete fillet units.

The contamination of the substrates in handling can lower the surface energy and wettability. Fig. 19

shows the contact angle of underfill for clean and contaminated substrates. The substrates with contamination have little spread and high contact angle. The average surface energies for the clean and contaminated substrates are 36.5 and 31 dyne/cm, respectively. Fig. 20 shows the effect of chip attach process on the surface energy of different substrates. After the chip attach process the surface energy increased.

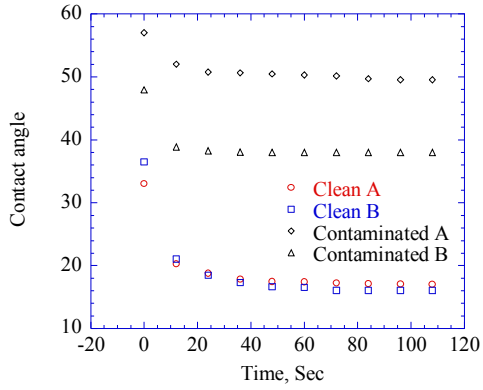

Fig. 19. The contact angle of underfill for clean and contaminated substrates.

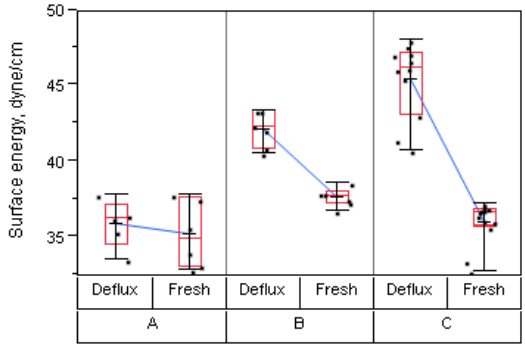

Fig.20. The effect of chip attach process on the surface energy of different substrates.

Fig. 21 shows the correlation between the surface energy of the substrate and the underfill contact angle. For high surface energy surfaces, the underfill has a good spread and a low contact angle.

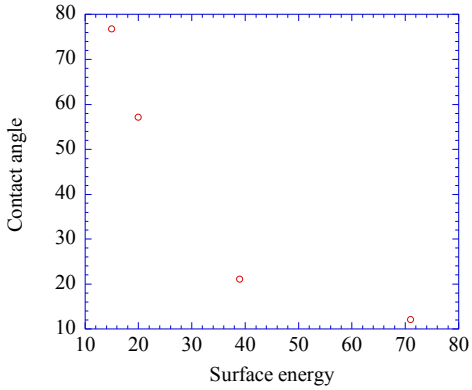

Fig. 21. shows the correlation between the surface energy and underfill contact angle.

Conclusions

Surface energy measurement provides a fast and convenient method for wettability analysis of solid surfaces. The work of adhesion for two solid surfaces was calculated from the surface energy components. The surface energy of substrates has good correlation with the flux and underfill contact angles. The surface energy methods also show some limitations. For certain measured contact angles, the surface energy either increases with contact angle or has a negative component. How to account the negative component in the total surface energy is still debatable and further study is needed. The substrate handling and assembly process affect its surface energy and wettability.

Acknowledgments

The author would like to thank Mark Nguyen for experimental assistance.

References

[1] M.K. Schwiebert and M.H. Leong, "Underfill Flow as Viscous Flow Between Parallel Plates Driven by Capillary Action", IEEE Transactions on Components, Packaging, and manufacturing Technology, Part C, Vol. 19, No2, pp. 133-137, April 1996.

[2] M. A. Rodriguez, et al., "Application of Inverse Gas Chromatography to the Study of the Surface Properties of Slates", Clays and Clay Minerals, Vol. 45, No. 5, 670-680, 1997.

[3] Jeahyeong Han, et al., "Surface energy approach and AFM verification of the (CF)n treated surface effect and its correlation with adhesion reduction in microvalves" J. Micromech. Microeng. Vol. 19, No. 8, pp 1-9, 2009.
[4] G.S. Ganesa, G. Lewis, and H.M. Berg, "Characterizing Organic Contamination in IC Package Assembly", International Journal of Microcircuits and Electronic Packaging, Vol. 17, No. 2, pp. 182-160, Second Quarter, 1994.
[5] R.A. Carpio, J.S. Pettersen, and D. Hudson, "Application of an Automated Contact Angle Measurement Instrument to Advanced Lithographic and Wafer Cleaning Progresses", 191st Meeting of the Electrochemical Society in Montreal, Canada, May 8, 1997.
[6] R.A. Carpio and D. Hudson, "The Quantification of Surface Modification in 200 and 300 mm Wafer Processing with an Automated Contact Angle System", 9th Annual Advanced Semiconductor Manufacturing Conference and Workshop, Boston, Massachusetts, September 24, 1998.
[7] S. Wu, Polymer Interface and Adhesion, pp. 327-334, Marcel Dekker, 1982.
[8] R.J. Good, "Contact Angle, Wetting, and Adhesion: a Critical Review", J. Adhesion Sci. Tech. Vol. 6, No. 12, pp. 1269-1302, 1992.
[9] F. Chen and W.V. Chang, "Applicability Study of a New Acid-Base Interaction Model in Polypeptides and Polyamides", Langmuir, Vol. 7, pp. 2401-2404, 1991.
[10] C. Della Volpe, et al, "The solid surface free energy calculation I. In defense of the multicomponent approach" Journal of Colloid and Interface Science, Vol. 271, pp 434–453, 2004.
[11] D. Y. Kwok, D. Li, and A. W. Neumann, "Evaluation of the Lifshitz-van der Waals/Acid-Base Approach To Determine Interfacial Tensions" Langmuir, Vol. 10, pp 1323-1328, 1994.
[12] Geelsu Hwang, Chang-Ha Lee, Ik-Sung Ahn, Byung Jin Mhin, "Determination of reliable Lewis acid–base surface tension components of a solid in LW–AB approach" Journal of Industrial and Engineering Chemistry, Vol. 17, pp 125–129, 2011.